2nd IFAC Workshop on Research, Education and Development of
Unmanned Aerial Systems
November 20-22, 2013. Compiegne, France

IFAC

Autonomous Landing of an Unmanned Aerial Vehicle using Image-Based Fuzzy Control

Miguel A. Olivares-Mendez [*] **Iván F. Mondragón** [**]
Pascual Campoy [***]

[*] *Automation Research group, Interdisciplinary Centre for Security,
Reliability and Trust (SnT), University of Luxembourg, Luxembourg
(e-mail: miguel.olivaresmendez@uni.lu)*
[**] *Pontificia Universidad Javeriana. Industrial Enginering
Department. Bogotá, Colombia
(email: imondragon@jveriana.edu.com)*
[***] *Computer Vision Group (CVG), Centro de Automatica y Robotica
(CAR), Universidad Politecnica de Madrid (UPM), Madrid, Spain
(e-mail: pascual.campoy@upm.es)*

Abstract: This paper presents a vision based autonomous landing control approach for unmanned aerial vehicles (UAV). The 3D position of an unmanned helicopter is estimated based on the homographies estimated of a known landmark. The translation and altitude estimation of the helicopter against the helipad position are the only information that is used to control the longitudinal, lateral and descend speeds of the vehicle. The control system approach consists in three Fuzzy controllers to manage the speeds of each 3D axis of the aircraft's coordinate system. The 3D position estimation was proven first, comparing it with the GPS + IMU data with very good results. The robust of the vision algorithm against occlusions was also tested. The excellent behavior of the Fuzzy control approach using the 3D position estimation based in homographies was proved in an outdoors test using a real unmanned helicopter.

Keywords: Fuzzy control, Computer vision, Aircraft control, Autonomous vehicle, Robot Navigation, Extended Kalman filters, Position estimation, Velocity control

1. INTRODUCTION

The unmanned aerial vehicles (UAV) have made its way quickly and decisively to the forefront of current aviation technology. Opportunities exist in a broadening number of fields for the application of UAV systems as the components of these systems become increasingly lighter and more powerful. Of particular interest are those occupations that require the execution of missions which depend heavily on dull, dirty, or dangerous work, UAVs provide a cheap, safe alternative to manned systems and often provide a far greater magnitude of capability. The big potential of the UAVs is used for a large number of civil applications, like surveillance, inspection, autonomous navigation, among others. This work is focused con the specific task of the autonomous landing. The are some works focused on the theoretical control part of this problem that have been checked in simulation environments like Cesetti et al. (2010) present a classical PID control using the SIFT vision algorithm, proving the feasibility of this algorithm for this specific task and testing the controllers in a simulated environment. De Wagter and Mulder (2005), the authors have evaluated the use of visual information at different stages of a UAV control system, including a visual controller and a pose estimation for autonomous landing using a chessboard pattern. In Fucen et al. (2009) a visual system is used to detect, identify a landing zone (helipad) and confirm the landing direction of the vehicle. Saripalli and Sukhatme (2007), Saripalli et al. (2003) proposed an experimental method for autonomous landing on a moving target, by tracking a known helipad and using it to complement the controller IMU+GPS state estimation. Some works have also present real tests with a VTOL aircraft like Saripalli et al. (2002) have developed a fusion sensor control system using GPS to localize the landmark, vision to track it, and sonars for the las three meters of the autonomous landing task. Merz et al. (2004), Merz et al. (2006), that use a method that fuses visual and inertial information in order to control an autonomous helicopter landing on known landmarks. Hermansson (2010) presents excellent results of an autonomous landing using fusion sensor (GPS, compass and vision) with a PID controller for track the landing location and land on a landmark.

Vision based landing for multi-rotor UAVs has been an actively studied field in recent years. Some examples are the work presented by Lange in Lange et al. (2008) where the visual system is used to estimate a vehicle position relative to a landing place. Voos (2009), Voos and Bou-Ammar (2010) propose a decomposition of a quadrotor control system in an outer-loop velocity control and an inner-loop attitude control system. In which the landing controller consists of a linear altitude controller and a

nonlinear 2D-tracking controller. Chitrakaran et al. (2005) present a deep theoretical work of a non-linear controller of a quadrotor that is built upon the homography-based techniques and Lyapunov design methods. Recently, Nonami et al. (2010) and then Wenzel Wenzel et al. (2011) have presented two different methods for small UAV autonomous takeoff, tracking and landing on a moving platform. The first is based on optical flow, the second uses IR landmarks visual tracking to estimate the aircraft position. Venugopalan et al. (2012) present very good results of an autonomous landing of a AR.Drone on a landing pad on a kayak.

In this work is presented a Fuzzy control vision-based approach for the autonomous landing task. This 3D position estimation of a VTOL aircraft is done using homographies of a know landmark or helipad. The Fuzzy control approach works without any information about the model of the system, managing the longitudinal and lateral speeds, and the altitude of the helicopter. The use of the homographies using Lucas-Kanade and RANSAC gets good results despite the occlusion of the detected landmark, being this method ideal for this specific task. The present Fuzzy control approach manage the low rate of the vision control loop of 8 Hz and the vibration of the camera to accomplish successfully real tests with a reduced RMSE value, and without using any other sensor.

The outline of this paper is organized as follows: Section 2 introduces the 3D position estimation based on homgraphies. Section 3 shows the longitudinal and lateral speeds, and the altitude controllers for the autonomous landing task. Section 4 presents the RC helicopter used, the tests of the 3D position estimation using homographies, and a real test of an autonomous landing. Conclusions and future work are presented in section 5.

2. 3D ESTIMATION BASED ON HOMOGRAPHIES

Next is explained how the frame-to-frame homography is estimated using matched points and robust model fitting algorithms. For it, the pyramidal Lucas-Kanade optical flow Bouguet Jean Yves (1999) on corners detected using the method of Shi and Tomasi Shi and Tomasi (1994) is used to generate a set of corresponding points, then, a RANSAC Fischer and Bolles (1981) algorithm is used to robustly estimate projective transformation between the reference object and the image. Next section explains how this frame-to-frame is used to obtain the 3D pose of the object with respect to the camera coordinate system.

On images with high motion, good matched features can be obtained using the well known Pyramidal Lucas-Kanade algorithm modification Bouguet Jean Yves (1999). It is used to solve the problem that arise when large and non-coherent motion are present between consecutive frames, by first tracking features over large spatial scales on the pyramid image, obtaining an initial motion estimation, and then refining it by down sampling the levels of the images pyramid until it arrives at the original scale.

The set of corresponding or matched points between two consecutive images $((x_i, y_i) \leftrightarrow (x'_i, y'_i)$ for $i = 1 \ldots n,)$ obtained using the pyramidal Lucas-Kanade optical flow is used to compute the 3x3 matrix $\mathbf{H}$ that takes each $\bar{\mathbf{x}}_i$ to $\bar{\mathbf{x}}'_i$ or $\bar{\mathbf{x}}'_i = \mathbf{H}\bar{\mathbf{x}}_i$ or the Homography that relates both images. The matched points often have two error sources. The first one is the measurement of the point position, which follows a Gaussian distribution. The second one is the *outliers* to the Gaussian error distribution, which are the mismatched points given by the selected algorithm. These outliers can severely disturb the estimated homography, and consequently alter any measurement based on homographies. In order to select a set of *inliers* from the total set of correspondences so that the homography can be estimated employing only the set of pairs considered as inliers, *robust estimation* using Random Sample Consensus (RANSAC) algorithm Fischer and Bolles (1981) is used. It achieves its goal by iteratively selecting a random subset of the original data points by testing it to obtain the model and evaluating the model consensus, which is the total number of original data points that best fit the model. In the case of a Homography, four correspondences are enough to have a exact solution or minimal solution using the Inhomogeneous method Criminisi et al. (1999). This procedure is then repeated a fixed number of times, each time producing either a model which is rejected because too few points are classified as inliers, or a refined model. When total trials are reached, the algorithm returns the Homography with the largest number of inlier.

2.1 World Plane Projection onto The Image Plane

In order to align the planar object on the world space and the camera axis system, we consider the general pinhole camera model and the homogeneous camera projection matrix, that maps a world point $\mathbf{x}_w$ in $\mathbb{P}^3$ to a point $\mathbf{x}^i$ on i^{th} image in $\mathbb{P}^2$, defined by equation 1:

$$s\mathbf{x}^i = \mathbf{P}^i\mathbf{x}_w = \mathbf{K}[\mathbf{R}^i|\mathbf{t}^i]\mathbf{x}_w = \mathbf{K}\left[\mathbf{r}_1^i\ \mathbf{r}_2^i\ \mathbf{r}_3^i\ \mathbf{t}^i\right]\mathbf{x}_w \quad (1)$$

where the matrix $\mathbf{K}$ is the camera calibration matrix, $\mathbf{R}^i$ and $\mathbf{t}^i$ are the rotation and translation that relates the world coordinate system and camera coordinate system, and s is an arbitrary scale factor. Figure 1 shows the relation between a world reference plane and two images taken by a moving camera, showing the homography induced by a plane between these two frames.
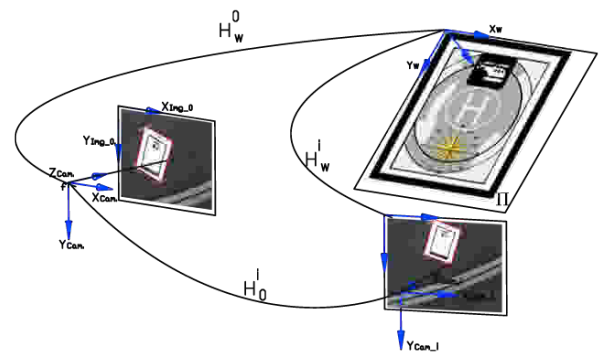

Fig. 1. Projection model on a moving camera and frame-to-frame homography induced by a plane.

If point $\mathbf{x}_w$ is restricted to lie on a plane Π , with a coordinate system selected in such a way that the plane equation of Π is $Z = 0$, the camera projection matrix can be written as equation 2:

$$sx^i = P^i x_\Pi = P^i \begin{bmatrix} X \\ Y \\ 0 \\ 1 \end{bmatrix} = \langle P^i \rangle \begin{bmatrix} X \\ Y \\ 1 \end{bmatrix} \qquad (2)$$

where $\langle P^i \rangle$ denotes that this matrix is deprived on its third column or $\langle P^i \rangle = K \left[r_1^i \ r_2^i \ t^i \right]$. The deprived camera projection matrix is a 3×3 projection matrix, which transforms points on the world plane (now in $\mathbb{P}^2$) to the ith image plane (likewise in $\mathbb{P}^2$), that is none other that a planar homography H_w^i defined up to scale factor as equation 3 shows.

$$H_w^i = K \left[r_1^i \ r_2^i \ t^i \right] = \langle P^i \rangle \qquad (3)$$

Equation 3 defines the homography which transforms points on the world plate to the ith image plane. Any point on the world plane $x_\Pi = [x_\Pi, y_\Pi, 1]^T$ is projected on the image plane as $x = [x, y, 1]^T$. Because the world plane coordinates system is not know for the ith image, H_w^i can not be directly evaluated. However, if the position of the word plane for a reference image is known, a homography H_w^0, can be defined. Then, the ith image can be related with the reference image to obtain the homography H_0^i. This mapping is obtained using sequential frame-to-frame homographies H_{i-1}^i, calculated for any pair of frames (i-1,i) and used to relate the ith frame to the first image H_0^i using equation 4:

$$H_0^i = H_{i-1}^i H_{i-2}^{i-1} \cdots H_0^1 \qquad (4)$$

This mapping and the aligning between initial frame to world plane reference is used to obtain the projection between the world plane and the ith image $H_w^i = H_0^i H_w^0$. In order to relate the world plane and the ith image, we must know the homography H_w^0. A simple method to obtain it, requires to match four points on the image with the corresponding corners of the rectangle in the scene, forming the matched points $(0,0) \leftrightarrow (x_1, y_1)$, $(0, \Pi_{Width}) \leftrightarrow (x_2, y_2)$, $(\Pi_{Lenght}, 0) \leftrightarrow (x_3, y_3)$ and $(\Pi_{Lenght}, \Pi_{Width}) \leftrightarrow (x_4, y_4)$. This process can be done by both, a helipad frame and corners detector or by an operator through a ground station interface. The helipad points selection generates a world plane defined in a coordinate frame in which the plane equation of Π is $Z = 0$. With these four correspondences between the world plane and the image plane, the minimal solution for homography $H_w^0 = \left[h_{1w}^0 \ h_{2w}^0 \ h_{3w}^0 \right]$ is obtained.

2.2 Translation Vector and Rotation Matrix

The rotation matrix and the translation vector are computed from the plane to image homography using the method described in Zhang (2000).

From equation 3 and defining the scale factor $\lambda = 1/s$, we have that

$$[r_1 \ r_2 \ t] = \lambda K^{-1} H_w^i = \lambda K^{-1} [h_1 \ h_2 \ h_3]$$
where
$$r_1 = \lambda K^{-1} h_1, \ r_2 = \lambda K^{-1} h_2, \ t = \lambda K^{-1} h_3 \qquad (5)$$

The scale factor is calculated as $\lambda = \frac{1}{\|K^{-1}h_1\|}$.

Because the columns of the rotation matrix must be orthonormal, the third vector of the rotation matrix r_3 could be determined by the cross product of $r_1 \times r_2$. However, the noise on the homography estimation causes that the resulting matrix $R = [r_1 \ r_2 \ r_3]$ does not satisfy the orthonormality condition and we must find a new rotation matrix R' that best approximates to the given matrix R according to smallest Frobenius norm for matrices (the root of the sum of squared matrix coefficients) Sturm (2000) Zhang (2000). As demonstrated by Zhang (2000), this problem can be solved by forming the Rotation Matrix $R = [r_1 \ r_2 \ (r_1 \times r_2)] = USV^T$ and using singular value decomposition (SVD) to form the new optimal rotation matrix $R' = UV^T$.

The solution for the camera pose problem is defined as $x^i = P^i X = K[R'|t]X$.

The translational vector obtained is already scaled based on the dimensions defined for the reference plane during the alignment between the helipad and image I_0, so if the dimensions of the world rectangle are defined in mm, the resulting vector $t_w^i = [x, y, z]^t$ is also in mm. In Mondragón et al. (2010), it is show how the Rotation Matrix can be decomposed in order to obtain the Tait-Bryan or Cardan Angles, which is one of the preferred rotation sequences in flight and vehicle dynamics. Specifically, these angles are formed by the sequence: (1) ψ about z axis (yaw $R_{z,\psi}$), (2) θ about y_a (pitch $R_{y,\theta}$), and (3) ϕ about the final x_b axis (roll $R_{x,\phi}$), where a and b denote the second and third stage in a three-stage sequence or axes.

2.3 Estimation Filtering.

An extended Kalman Filter (EKF) has been incorporated in the 3D pose estimation algorithm in order to smooth the position and correct the errors caused by the homography drift along time. The state vector is defined as the position $[x_k, y_k, z_k]$ and velocity $[\Delta x_k, \Delta y_k, \Delta z_k]$ of the kth helipad expressed in the onboard camera coordinate system. We consider the dynamic model as a linear system with constant velocity, as presented in the following equations:

$$x_k = F x_{k-1} + w_k \qquad (6)$$

$$\begin{bmatrix} x_k \\ y_k \\ z_k \\ \Delta x_k \\ \Delta y_k \\ \Delta z_k \end{bmatrix} = \begin{bmatrix} 1 & 0 & 0 & \Delta t & 0 & 0 \\ 0 & 1 & 0 & 0 & \Delta t & 0 \\ 0 & 0 & 1 & 0 & 0 & \Delta t \\ 0 & 0 & 0 & 1 & 0 & 0 \\ 0 & 0 & 0 & 0 & 1 & 0 \\ 0 & 0 & 0 & 0 & 0 & 1 \end{bmatrix} \begin{bmatrix} x_{k-1} \\ y_{k-1} \\ z_{k-1} \\ \Delta x_{k-1} \\ \Delta y_{k-1} \\ \Delta z_{k-1} \end{bmatrix} \qquad (7)$$
$$+ w_{t-1}$$

Where x_{k-1} is the state vector (position and velocity), F is the system matrix, w the process noise, and Δt represents the time step.

Because the visual system only estimates the position of the helipad, the measurements are expressed as follows:

$$z_k = \begin{bmatrix} \bar{x}_k \\ \bar{y}_k \\ \bar{z}_k \end{bmatrix} + v_k \qquad (8)$$

Where z_k is the measurement vector and $[\bar{x}_k, \bar{y}_k, \bar{z}_k]^t$ is the position of the helipad with respect to the camera

coordinate system and $\mathbf{v_k}$ is measurement noise . With the previous definitions, the two phases of the filter Prediction and Correction can be formulated as presented in Welch and Bishop (1995), assuming that the process noise $\mathbf{w_k}$ and the measurement noise $\mathbf{v_k}$ are white, zero-mean, Gaussian noise with covariance matrix $\mathbf{Q}$ and $\mathbf{R}$, respectively. The output of the filter is the smoothed position of the helipad, that will be used as input for the control system.

This method is similar to the one propose by Simon et al. (2000), Simon and Berger (2002) and is deeply detailed in Mondragón et al. (2010)

3. FUZZY CONTROL APPROACH FOR AUTONOMOUS LANDING

Three controllers were design to control the aircraft for the autolanding task. All of these controllers were developed using the software MOFS (Miguel Olivares' Fuzzy Software). The three developed controllers have as inputs the homography estimation of the altitude, the lateral and the longitudinal errors. The controllers commands the thrust, and lateral and longitudinal speeds of the UAV. The altitude controller was developed first independently and tested Olivares-Mendez et al. (2010). After checking the correct behavior of this controller, we design the lateral and longitudinal speeds controller for a complete control for the autonomous landing task. The three controllers were defined as PD-like. The design of the membership function of the controller was done using triangular membership functions, based on the good results obtained in the previous works of the authors. The definition of the variables' sets and the rules' base is based on heuristic information. This data was acquired from different manual and hover flight tests over the helipad.

The control system is based on the camera configuration, like a eye-to-hand configuration, because the camera is fixed on the UAV. The position of the camera with respect to the robot, follows an eye-in-hand type. The architecture of the visual and servo system is a dynamic look-and-move system, that sends velocity commands.

The thrust controller was implemented for control the altitude of the UAV during the autolanding task (Figure 2). It was design with two inputs and one output. The two inputs are: the estimation of the altitude, that is made by the homography (Figure 2(a)), and the derivate of this value (Figure 2(b)). The output of the controller is the velocity command, in meters per second, that is executed by the aircraft to descend to the helipad location (Figure 2(c)).

The lateral and longitudinal speed controllers are quite similar, the only thing that changes is the linguistic value of the membership functions' sets. As well as the thrust controller these controllers have a PD-like definition. The lateral speed controller is shown in Figure 3. The first input is the lateral error estimation using the 3D position estimation of the homography (Figure 3(a)). The second input is the derivate of this error (Figure 3(b)). The output of the controllers is the lateral speed command in m/s to sent to the UAV (Figure 3(c)).
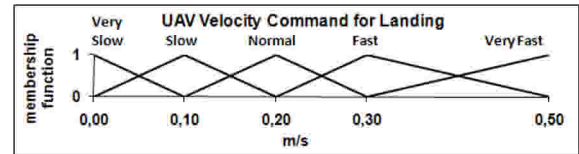
The longitudinal speed controller is shown in Figure 4. The first input is the front/back error estimation using the 3D
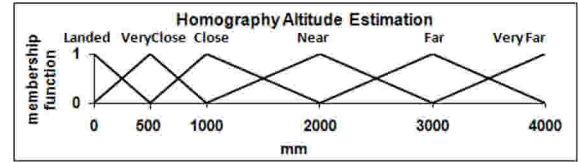
(a) Estimation of the altitude (mm), based on the homography of the helipad.
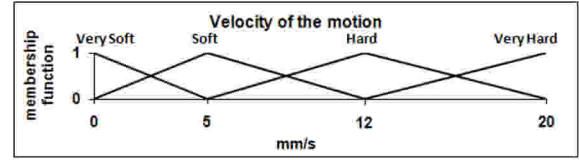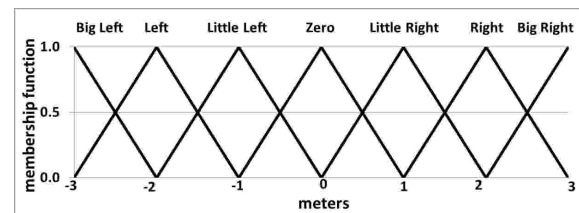

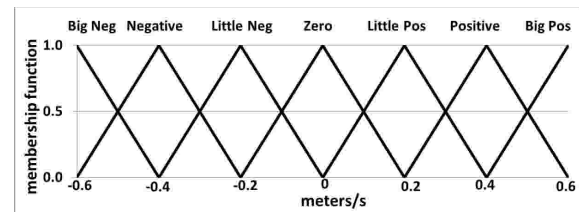(b) Derivate of the altitude estimation (mm/s).

(c) Output of the Fuzzy Controller, velocity commands for the UAV's thrust in m/s.
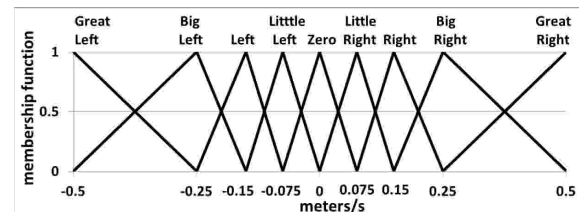
Fig. 2. Fuzzy controller for UAV's altitude.

(a) Estimation of the lateral error (m), based on the homography of the helipad.
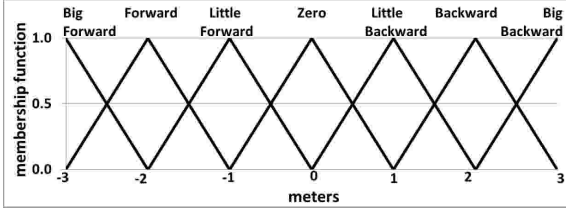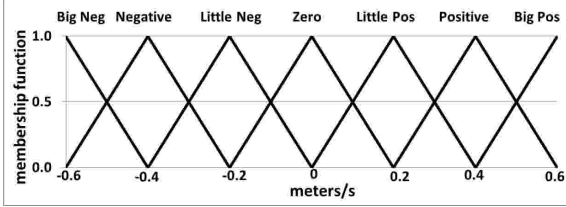

(b) Derivate of the lateral error (m/s).

(c) Output of the Fuzzy Controller, velocity commands for the UAV's lateral speed in m/s.

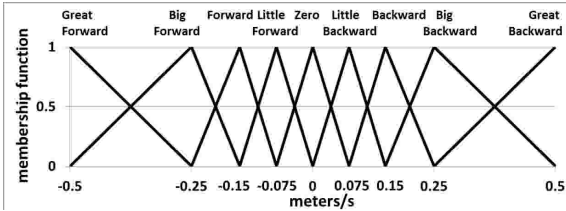Fig. 3. Fuzzy controller for UAV's lateral speed.

position estimation of the homography (Figure 4(a)). The second input is the derivate of this error (Figure 3(b)). The output of the controllers is the longitudinal speed command in m/s to sent to the UAV (Figure 4(c)).

(a) Estimation of the front/back error (m), based on the homography of the helipad.

(b) Derivate of the front/back error (m/s).

(c) Output of the Fuzzy Controller, velocity commands for the UAV's longitudinal speed in m/s.

Fig. 4. Fuzzy controller for UAV's longitudinal speed.

The product t-norm is used for rules conjunction. Since rule weights will be optimized with CE method, the defuzzification method used in this approach is a modification of the height method. We introduce the value of the weight assigned to each rule in the defuzzification process. Equation 9 shows the defuzzification method.

$$y = \frac{\sum_{l=1}^{M} \overline{y}^l \prod_{i=1}^{N} \left(\mu_{x_i^l}(x_i) \right)}{\sum_{l=1}^{M} \prod_{i=1}^{N} \left(\mu_{x_i^l}(x_i) \right)} \qquad (9)$$

Where N and M represent the number of inputs variables and total number of rules respectively. $\mu_{x_i^l}$ denote the membership function of the lth rule for the ith input variable. $\overline{y}^l$ represent the output of the lth rule.

4. EXPERIMENTS

4.1 UAV platform

To test the Fuzzy control approach and the 3D position estimation for the autonomous landing task a real RC helicopter has been used. This aircraft is an electric helicopter SR20, shown in Figure 5. This is a modified Xcell Electric RC helicopter.

This aircraft is equipped with an Xscale-based flight computer augmented with sensors (GPS, IMU, Magnetometer, fused with a Kalman filter for state estimation). Additionally it has a VIA mini-ITX 1.5 GHz onboard computer with 2 Gb RAM, a wireless interface. The system runs in a client-server architecture using TCP/UDP messages
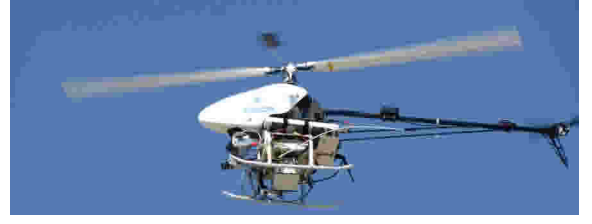

Fig. 5. Autonomous electric helicopter SR20.

with Ubuntu Linux OS working in a multi-client wireless 802.11g ad-hoc network, allowing the integration of vision systems and vision tasks with the flight control. This architecture allows embedded applications to run onboard the autonomous helicopter while it interacts with external processes through a high level switching layer. The visual control system and additional external processes are also integrated with the flight control through this layer using TCP/UDP messages. The layer is based on a communications API where all messages and data types are defined.

The selected vision sensor used is a Monocromo CCD Firewire camera with a resolution of $640x480$ pixels is used. The camera is calibrated before each test, so the intrinsic parameters are known. The camera is installed in such a way that it is looking downward with relation to the UAV. A rectangular helipad with known measures is used as the reference object to estimate the 3D position of the UAV. It is aligned in such a way that its axes are parallel to the local plane North East axes. This helipad was designed in such a way that it produces many distinctive corners for the visual tracking. Figure 6, shows the helipad used and the coordinate systems involved in the pose estimation.
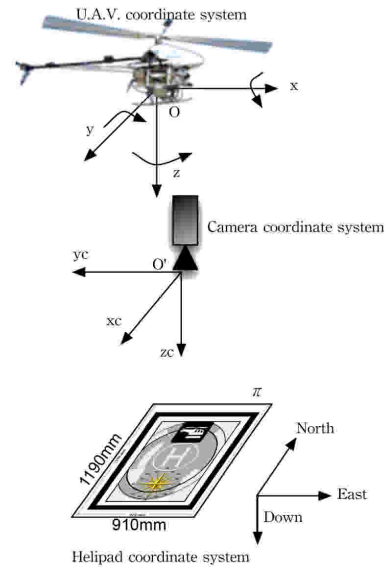

Fig. 6. Helipad, camera and U.A.V coordinate systems

Figure 7 shows the control loop designed for the Fuzzy control approach using vision for this specific task. In this Figure it can be seen that the UAV has internal control loops for the stability of the system, based on the IMu and GPS information. The presented control approach is a external control loop based on vision that works at 8 Hz, it means that the system process 8 frames per seconds.
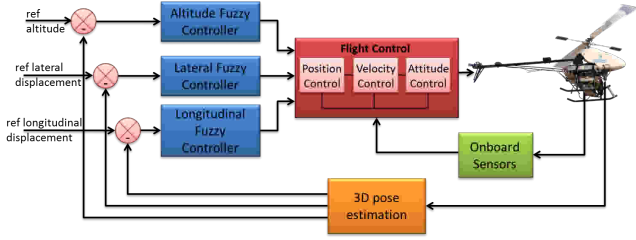
Fig. 7. Control Loop for the autonomous landing task.

4.2 Tests of the 3D Position Estimation

Next are presented the position estimation tests based on the homography. The test begins when the UAV is hovering over the helipad, a moment in which the helipad is detected, tracked and used for estimating the 3D position of landmark w.r.t aircraft. One test begins at 4.2 meters of altitude and the other test at 10 meters. The estimated 3D position is compared with helicopter position estimated by the autopilot (IMU+GPS data) on the local plane with reference to the takeoff point (center of the Helipad). Because the local tangent plane to the helicopter is defined in such a way that the X axis is the North position, the Y axis is the East position and Z axis is the Down Position (negative), the Measured X and Y values must be rotated according with the helicopter heading or Yaw angle, in order to be comparable with the estimated values obtaining from the homographies. Figures 8, 9 and 10 shows the landmark position with respect to the UAV
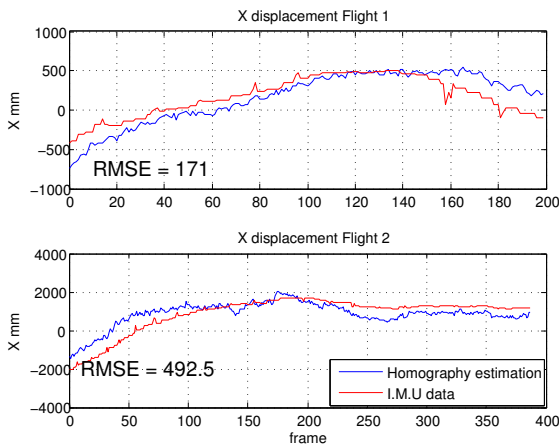

Fig. 8. Measures of the X axis of the UAV (Roll) based on the homography estimation.

Results show a good performance of the visual values compared with the IMU+GPS state estimated data. In general, estimated and state estimation data have the same behavior for both test sequences. For X and Y, there is a small error between the aircraft pose state and the values estimated using the visual system, giving a maximum root mean squared error RMSE of 0.42 m in X axis and 0.16 m in Y axis. The estimated altitude position Z have a small error for flight 1 with a RMSE of 0.16 m and 0.85 m in test 2. Although results are good for height estimation, is important to remember that the state altitude estimation has an accuracy of ± 0.5 m, causing that the reference altitude estimation used to validate our approach have a big uncertainty. Finally, the Yaw angle is correctly estimated,
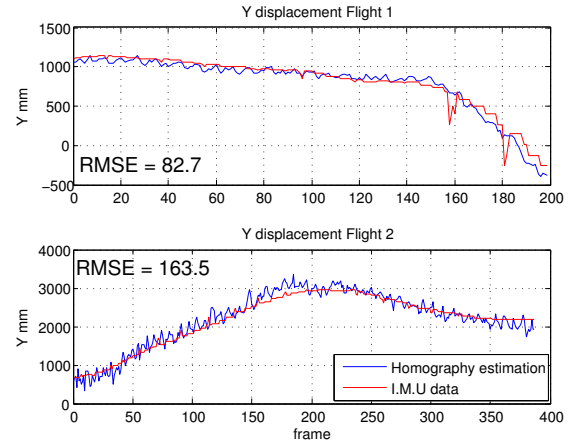

Fig. 9. Measures of the Y axis of the UAV (Pitch) based on the homography estimation.
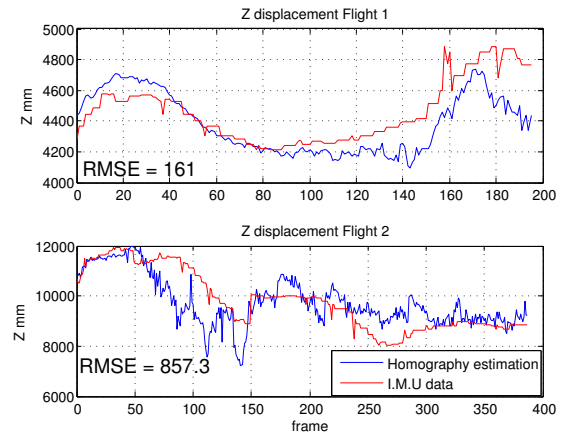

Fig. 10. Measures of the altitude of the UAV based on the homography estimation.

presenting for the first flight and error of 2° between the IMU and the estimated data, and 4° for the second tests.

Results have also shown that the system correctly estimate the 3D position when a maximum of the 70 % of the landmark is partially occluded or out of the camera field of view as Figure 11 shows.

4.3 Real tests

For the autonomous landing test the helicopter is take off and flight initially by remote control. During all the test is possible to see the camera onboard image in the ground station. When the aircraft has an altitude around four meters and the helipad is in the field of view of the camera, it is selected autonomously and the image processing starts. The longitudinal and lateral controllers are working during all the time that the image processing is activated. But, the altitude controller works only when the lateral and longitudinal errors are lower than a fixed value, it means when the helipad is centered in the image. Furthermore, the altitude controller will stops when the UAV's altitude estimation is lower than 1.5 meters, reducing the power of the motor to finish the landing task.
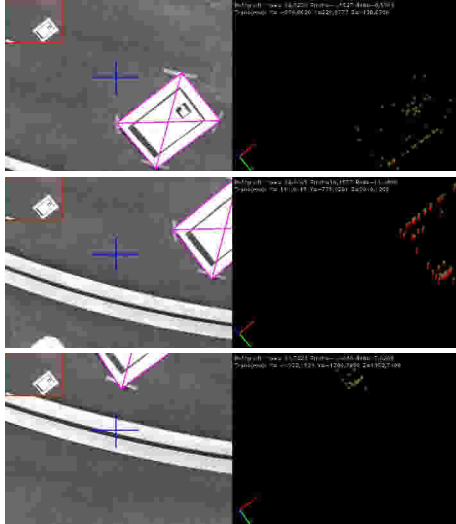
Fig. 11. 3D pose estimation occlusion robustness. The system correctly estimate the 3D position when a maximum of the 70 % of the landmark is partially occluded or out of the camera field of view.

Figure 12 shows the 3D reconstruction of the autonomous landing test using the GPS data. Figure 13 shows the measured done using the 3D positioning based on the homography estimation for longitudinal and lateral errors, and the altitude estimation. In this flight the autonomous landing start at 4 meters. The RMSE value for the longitudinal measures in this experiment is 0.7344 meters and for the lateral measures is 0.7199.
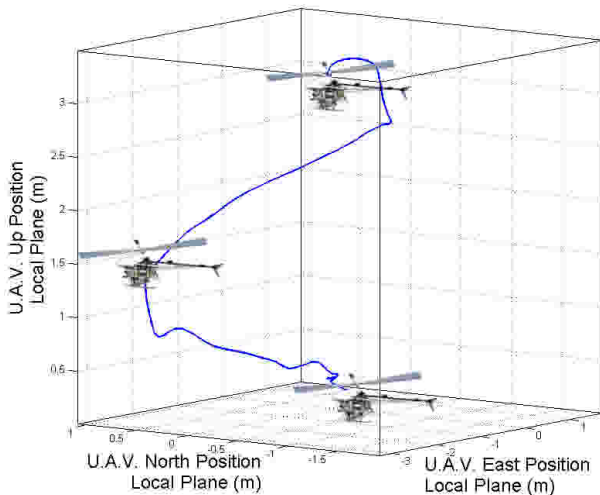

Fig. 12. 3D flight reconstruction of a fully autonomous landing test.

The autonomous landing task was accomplish successfully with the controller and vision approach developed in this work. The value of the RMSE in the lateral and the longitudinal errors are inside a comprehensive limits taking into account the high vibration of the aircraft and the delay of the response on this type of system and the high sensibility to wind disturbances of a VTOL.

Some videos related to this work could be found at M. A. Olivares-Mendez (2013).
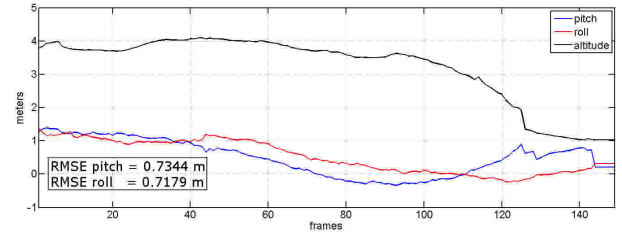

Fig. 13. Homography estimation for longitudinal and lateral error, and altitude estimation for a fully autonomous landing.

5. CONCLUSIONS AND FUTURE WORK

In this work is presented a Fuzzy control approach to manage the longitudinal and lateral speeds, and the altitude of an unmanned aerial vehicle using vision for the autonomous landing task. An unmanned helicopter with a downward camera was used for this specific task. The image processing is done in a onboard computer, and estimate the position of the UAV based on the homography estimation of a know helipad. This information is filtered by an extended Kalman filter, and then is sent to the control system to keep the helipad centered in the image by the longitudinal and lateral speed controllers, and to land on it by the altitude controller. The high vibrations of the UAV that are propagated to the fixed downward camera affects the estimation of the position done by the image processing algorithm, but are manage in a gentle way by the Fuzzy control approach to accomplish the task successfully with a reduced RMSE. value.

After accomplish the autonomous landing task with a static helipad the next step to do is to land on a ground moving target, and continue with a ship. To increase the accuracy of the estimation, the authors are working on fusion other senors like a laser.

REFERENCES

Bouguet Jean Yves (1999). Pyramidal implementation of the lucas-kanade feature tracker. Technical report, Intel Corporation. Microprocessor Research Labs, Santa Clara, CA 95052.

Cesetti, A., Frontoni, E., Mancini, A., Zingaretti, P., and Longhi, S. (2010). A vision-based guidance system for uav navigation and safe landing using natural landmarks. *Journal of Intelligent and Robotic Systems*, 57(1-4), 233–257.

Chitrakaran, V., Dawson, D., Chen, J., and Feemster, M. (2005). Vision assisted autonomous landing of an unmanned aerial vehicle. In *Decision and Control, 2005 and 2005 European Control Conference. CDC-ECC '05. 44th IEEE Conference on*, 1465–1470. doi:10.1109/CDC.2005.1582365.

Criminisi, A., Reid, I.D., and Zisserman, A. (1999). A plane measuring device. *Image Vision Comput.*, 17(8), 625–634.

De Wagter, C. and Mulder, J. (2005). Towards vision-based uav situation awareness. *AIAA Guidance, Navigation, and Control Conference and Exhibit.*

Fischer, M.A. and Bolles, R.C. (1981). Random sample concensus: a paradigm for model fitting with applications to image analysis and automated cartography. *Communications of the ACM*, 24(6), 381–395.

Fucen, Z., Haiqing, S., and Hong, W. (2009). The object recognition and adaptive threshold selection in the vision system for landing an unmanned aerial vehicle. In *Information and Automation, 2009. ICIA '09. International Conference on*, 117 –122. doi:10.1109/ICINFA.2009.5204904.

Hermansson, J. (2010). *Vision and GPS based autonomous landing of an unmanned aerial vehicle*. Ph.D. thesis, Linkping University, Department of Electrical Engineering, Automatic Control, Sweeden.

Lange, S., Sünderhauf, N., and Protzel, P. (2008). Autonomous landing for a multirotor UAV using vision. In *In Workshop Proceedings of SIMPAR Intl. Conf. on SIMULATION, MODELING and PROGRAMMING for AUTONOMOUS ROBOTS*, 482–491. Venice, Italy.

M. A. Olivares-Mendez, I. Mondragon, P.C. (2013). Autonomous landing of an unmanned aerial vehicle using image-based fuzzy control. test videos. `www.vision4uav.eu/?q=researchline/autonomousLanding_REDUAS13`. Computer Vision Group. Polytechnic University of Madrid.

Merz, T., Duranti, S., and Conte, G. (2004). Autonomous landing of an unmanned helicopter based on vision and inbertial sensing. In *International Symposium on Experimental Robotics*. Singapore.

Merz, T., Duranti, S., and Conte, G. (2006). Autonomous landing of an unmanned helicopter based on vision and inertial sensing. In M. Ang and O. Khatib (eds.), *Experimental Robotics IX*, volume 21 of *Springer Tracts in Advanced Robotics*, 343–352. Springer Berlin / Heidelberg.

Mondragón, I.F., Campoy, P., Martínez, C., and Olivares-Méndez, M. (2010). 3d pose estimation based on planar object tracking for UAVs control. In *Robotics and Automation (ICRA), 2010 IEEE International Conference on*, 35 –41. doi:10.1109/ROBOT.2010.5509287.

Nonami, K., Kendoul, F., Suzuki, S., Wang, W., and Nakazawa, D. (2010). Guidance and navigation systems for small aerial robots. In *Autonomous Flying Robots*, 219–250. Springer Japan.

Olivares-Mendez, M., Mondragon, I., Campoy, P., and Martinez, C. (2010). Fuzzy controller for uav-landing task using 3d-position visual estimation. In *Fuzzy Systems (FUZZ), 2010 IEEE International Conference on*, 1–8. doi:10.1109/FUZZY.2010.5584396.

Saripalli, S., Montgomery, J., and Sukhatme, G. (2002). Vision-based autonomous landing of an unmanned aerial vehicle. In *Robotics and Automation, 2002. Proceedings. ICRA '02. IEEE International Conference on*, volume 3, 2799 –2804. doi:10.1109/ROBOT.2002.1013656.

Saripalli, S., Montgomery, J.F., and Sukhatme, G.S. (2003). Visually-guided landing of an unmanned aerial vehicle. *IEEE Transactions on Robotics and Automation*, 19(3), 371–381.

Saripalli, S. and Sukhatme, G.S. (2007). Landing a helicopter on a moving target. In *Proceedings of IEEE International Conference on Robotics and Automation*, 2030–2035. Rome, Italy.

Shi, J. and Tomasi, C. (1994). Good features to track. In *1994 IEEE Conference on Computer Vision and Pattern Recognition (CVPR'94)*, 593–600.

Simon, G., Fitzgibbon, A., and Zisserman, A. (2000). Markerless tracking using planar structures in the scene. In *Augmented Reality, 2000. (ISAR 2000). Proceedings. IEEE and ACM International Symposium on*, 120–128. doi:10.1109/ISAR.2000.880935.

Simon, G. and Berger, M.O. (2002). Pose estimation for planar structures. *Computer Graphics and Applications, IEEE*, 22(6), 46–53. doi:10.1109/MCG.2002.1046628.

Sturm, P. (2000). Algorithms for plane-based pose estimation. In *Proceedings of the IEEE Conference on Computer Vision and Pattern Recognition, Hilton Head Island, South Carolina, USA*, 1010–1017.

Venugopalan, T., Taher, T., and Barbastathis, G. (2012). Autonomous landing of an unmanned aerial vehicle on an autonomous marine vehicle. In *Oceans, 2012*, 1–9.

Voos, H. (2009). Nonlinear landing control for quadrotor uavs. In R. Dillmann, J. Beyerer, C. Stiller, J. Zllner, and T. Gindele (eds.), *Autonome Mobile Systeme 2009*, Informatik aktuell, 113–120. Springer Berlin Heidelberg.

Voos, H. and Bou-Ammar, H. (2010). Nonlinear tracking and landing controller for quadrotor aerial robots. In *CCA*, 2136–2141.

Welch, G. and Bishop, G. (1995). An introduction to the kalman filter. Technical report, University of North Carolina at Chapel Hill, Chapel Hill, NC, USA.

Wenzel, K., Masselli, A., and Zell, A. (2011). Automatic take off, tracking and landing of a miniature uav on a moving carrier vehicle. *Journal of Intelligent and Robotic Systems*, 61, 221–238. doi:10.1007/s10846-010-9473-0.

Zhang, Z. (2000). A flexible new technique for camera calibration. *IEEE Transactions on pattern analysis and machine intelligence*, 22(11), 1330–1334.